3-2021

Osteogenic Differentiation of Adipose-Derived Mesenchymal Stem Cells Using 3D-Printed PDLLA/ β-TCP Nanocomposite Scaffolds

Ashkan Bigham
Isfahan University of Medical Sciences

Amir Hamed Aghajanian
Isfahan University of Medical Sciences

Mehdi Movahedi
Islamic Azad University

Mansoureh Sattary
Isfahan University of Medical Sciences

Mohammad Rafienia
Isfahan University of Medical Sciences

See next page for additional authors

Bioprinting, Vol. 21 (March 2021): e00117. DOI.

Osteogenic Differentiation of Adipose-Derived Mesenchymal Stem Cells Using 3D-Printed PDLLA/ β-TCP Nanocomposite Scaffolds

Ashkan Bigham
Medical Image and Signal Processing Research Center, School of Advanced Technologies in Medicine, Isfahan University of Medical Sciences, Isfahan, Iran
Department of Biomaterials, Tissue Engineering and Nanotechnology, School of Advanced Technologies in Medicine (ATiM), Isfahan University of Medical Sciences, Isfahan, Iran
Amir Hamed Aghajanian
Department of Biomaterials, Tissue Engineering and Nanotechnology, School of Advanced Technologies in Medicine (ATiM), Isfahan University of Medical Sciences, Isfahan, Iran
Mehdi Movahedi
Biomedical Engineering (Biomaterials) Department, Islamic Azad University - Science and Research Branch, Tehran, Iran
Mansoureh Sattary
Department of Biomaterials, Tissue Engineering and Nanotechnology, School of Advanced Technologies in Medicine (ATiM), Isfahan University of Medical Sciences, Isfahan, Iran

Mohammad Rafienia
Biosensor Research Center, Isfahan University of Medical Sciences, Isfahan, Iran
Lobat Tayebi
Marquette University School of Dentistry, Milwaukee, WI

Abstract

Designing bone scaffolds containing both organic and inorganic composites simulating the architecture of the bone is the most important principle in bone tissue engineering. The objective of this study was to fabricate a composite scaffold containing poly (D, l)-lactide (PDLLA) and β-tricalcium phosphate (β-TCP) as a platform for osteogenic differentiation of adipose-derived mesenchymal stem cells. In this study, PDLLA/β-TCP scaffolds were fabricated using three-dimensional printing (3D) technology through melt excursion technique. The physicomechanical characteristics, including microstructure, mechanical properties, of the customized scaffolds were investigated. Further, the in vitro biological characteristics of manufactured scaffolds were evaluated in conjugation with buccal fat pad derived mesenchymal stem cells in terms of cell attachment, viability, proliferation, and osteogenic differentiation capacity. The 3D printed customized scaffold in this study showed proper pore size, porosity, mechanical strength, material composition, biocompatibility, and osteogenic differentiation capacity. The obtained results converge to reveal the promising features of the nanocomposite 3D printed platform for personalized bone tissue engineering.

Keywords

3D-printing, Mesenchymal stem cells, Buccal fat pad, Bone tissue engineering

1. Introduction

Designing bone scaffolds mimicking the natural structure of bone tissues is the most important principle in bone tissue engineering. The synthesis of scaffold containing both organic and inorganic composites simulating the architecture of the bone, which can be regarded as a polymer and ceramic composites, has been extensively investigated by several studies [1].The absorbable polymers lactic acid-based, such as poly(D, l)-lactide (PDLLA), have been widely used, which is due to their biodegradability and biocompatibility [[2], [3], [4], [5]]. However, the relatively low mechanical properties of pure polymer makes them improper for reconstruction of load-bearing areas [6,7]. Besides, the degradation of PDLLA creates the acidic environment next to the implant site which results in inflammatory reactions and prevents a complete degradation of the implant [2,5,8]. The β-tricalcium phosphate (β-TCP) is one of the most comprehensively investigated biocompatible ceramics that used in medical applications [2,4,9]. Studies have shown that β-TCP is a biocompatible and osteoconductive material with bone bonding capacity but have a limited degradability [4,[10], [11], [12], [13], [14], [15]].

Hence, the combing these materials would be beneficial in such each component has a specific function [2,3,16]. Studies have shown that incorporation of bioceramic, β-TCP, with polymer, PDLLA, lead to composite scaffold having improved mechanical properties as well as controllable degradation rates [3,17]. However, various percentage of β-TCP has been used in corporation with PDLLA in composite scaffolds [[2], [3], [4],18]. Despite the effect of ceramic materials in enhancement of mechanical properties of a composite scaffold as well as their significant effect in promotion of bone regeneration [3], lower percentage of ceramic component lead to fabricate a scaffold with desirable degradation rates [18,19].

Apart from scaffold materials, shape and microstructure of a scaffold is highly important. Various studies have shown that the appropriate bone healing is the result of the osseointegration between bone and scaffolds which

in turn is the consequence of matching the bone graft with defect [2,9]. The new additive manufacturing technologies including three-dimensional printing (3D), lead to design and fabricate of a scaffold matching desirable individual shape and proper internal structures [[20], [21], [22]]. Comparing to conventional methods, porous scaffolds could be fabricated like bone structure to create the porosity and interconnected pores [9,17]. Interconnected pores allow nutrients and molecules to transport to inner parts of a scaffold to facilitate cell migration, cell ingrowth, vascularization, continuous ingrowth of bone tissue, as well as waste material removal [4,23,24].

Given that, the objective of this study was to fabricate a composite scaffold containing PDLLA and β-TCP using a 3DP technology with the lower percentage of β-TCP (40% β-TCP vs 60% PDLLA), which has been less studied before. Then, the fabricated scaffolds, were first characterized for their physicomechanical properties in order to evaluate if their properties match natural bone structure. Secondly, their biological properties, including biocompatibility and osteogenic differentiation, were investigated after loading with adipose-derived mesenchymal stem cells from buccal fat pad (BFPSCs), in order to investigate the possible application in preclinical bone regeneration application.

2. Materials and methods

2.1. Fabrication of PDLLA and PDLLA/ß-TCP scaffolds by 3D printing

PDLLA/β-TCP composite was prepared using solvent casting method. Briefly, 2g PDLLA (PURASORB, Corbion) was dissolved in 20 ml Dichloromethane (Alfa Aesar), and 600 mg β-TCP (Sigma-Aldrich) was then added to the polymer solution and stirred using a magnet-stirrer for 2 h. The resultant mixture was then cast onto clean petri dishes and dried at room temperature. Finally, the cast PDLLA/β-TCP 30 wt% films were incubated overnight in a vacuum oven to be fully dried.

PDLLA and PDLLA/β-TCP scaffolds were printed through the melt extrusion technique using a commercial bioprinting system (3D-Bioplotter Manufacturer Series, EnvisionTEC). PDLLA and PDLLA/β-TCP composites were loaded in a steel cylinder which was sealed and inserted into a high temperature head of the machine. The system was purged and pressurized with nitrogen stream. The temperature of the head was set to 170°C and incubated for 10 min prior printing to be equilibrated. Scaffolds with square block models of $7 \times 7 \times 7$ mm^3 were designed using the Bioplotter CAD/CAM software (EnvisionTEC) Scaffolds were printed layer-by-layer with 0.8 mm distance between strands and a 90- degree shift between layers extruded from a nozzle with 0.4 mm inner diameter.

The pressure and dispensing speed were optimized at 2.0 bar, 5 mm/s and 2.5 bar, 4 mm/s for PDLLA and PDLLA/β-TCP scaffolds, respectively. It should be noticed that the pressure and speed of printing for PDLLA and PDLLA/β-TCP scaffolds were adjusted to achieve scaffolds with similar microstructure and pore size.

2.2. Physicomechanical characterization

2.2.1. Fourier transform infrared spectroscopy (FTIR) analysis

PDLLA/β-TCP composite scaffolds were characterized using a Nicolet™ iS5 FTIR Spectrometer (iD5 Diamond Attenuated total reflection) with the scan number of 16 and resolution of 4 cm^{-1}. Samples were analyzed in 4000–550 cm^{-1} wavenumber range and transmittance mode.

2.2.2. Differential scanning calorimetry (DSC) analysis

The thermal properties of PDLLA and PDLLA/β-TCP scaffolds were investigated by differential scanning calorimetry method (DSC, NETZSCH DSC 404F1 Pegasus®) All measurements were carried out with about 10 mg sample in aluminum crucibles with pierced lid under ultra-pure argon flow of 20 ml min^{-1} with the heating rate

of 10 °C min^{-1}. Prior to DSC measurements, samples were first heated up to 70 °C at the rate of 10 °C min^{-1}, and then cooled down to room temperature at the rate of 3 °C min^{-1}.

2.2.3. Evaluation of mechanical properties

Mechanical properties of fabricated scaffolds were determined at 25 °C in compression mode using a universal testing machine (AGS-X series, Shimadzu, Japan) with a 5 KN load cell at a speed of 1 mm/min. The samples (n = 5) with the size of 7 × 7 × 14 (W × L × H) mm^3 were compressed in Z direction. The compression was continued until the samples were fractured. Elastic moduli were derived from the initial linear region of the stress–strain curves.

2.2.4. Pore size measurement

The size of pores in 3D printed scaffolds (n = 3) was measured by means of laser scanning microscopy. The 3D printed PDLLA and PDLLA/β-TCP scaffolds were scanned for their microstructure using the LEXT OLS4000 3D Laser Measuring Microscope (Olympus LEXT OLS 4000, Japan)

2.2.5. Porosity measurement

The porosity of scaffolds was measured based on liquid displacement method [[25], [26], [27]]. In brief, scaffold specimens were first weighed (W_i), and then immersed in a predetermined volume of ethanol (V_1) at 25 °C for 10 min to ensure complete wetting. Subsequently, the volume of the ethanol after immersion of the scaffold was measured (V_2) to calculate the volume of the scaffold (V_2–V_1). Based on the initial (W_i) and final (W_f) weights of the scaffolds after soaking in ethanol, the pore volume of scaffolds can be achieved as (Wf−Wi)/ρethanoland the porosity can be calculated using the following equation,Porosity=(Wf−Wi)/ρethanolV2−V1

2.3. Biocompatibility evaluation

2.3.1. Establishment of BFPSC cultures and their characterization according to international society for cellular therapy (ISCT) criteria

Buccal fat pad tissues were harvested from vestibular incision distal to the maxillary second molar of healthy volunteers. The tissues were digested in a solution of 3 mg/ml type I collagenase for 1 h at 37°C. Then, the cells were re-suspended in stem cell growth medium containing Dulbecco's Modified Eagle's medium (DMEM, Thermo Fisher Scientific) supplemented with 15% Fetal Bovine Serum (FBS, Thermo Fisher Scientific) and 1% penicillin/Streptomycin (Life Technologies) and cultured in T-25 flasks under 5% CO2 at 37°C. The cells were sub-cultured at 80% confluency using 0.25% trypsin-EDTA (Life Technologies) at a ratio of 1:3 until desired passage (P3)was obtained.

In order to confirm whether the isolated/cultured BFPSCs display the Mesenchymal Stem Cell (MSC) phenotype, the cells were subjected to flow cytometry analysis for expression of positive (CD44, CD90, CD73 and CD105) and negative (CD45 and CD34) MSC markers. Briefly, cells at P3 were treated with 0.05% trypsin-EDTA. The harvested cells were centrifuged and then, cell pellets were re-suspended at concentration of 105 per sample in PBS and incubated for 30 min at 4°C in the dark room with antibodies. After incubation time, cells were washed with Phosphate-Buffered Saline (PBS, Sigma-Aldrich). Analysis was next performed using flow cytometer (Applied Biosystems). The positive control expression was defined as the level of fluorescence greater than 99% of the corresponding unstained cells.

Moreover, the multilineage differentiation capability of BFPSCs was also evaluated. To do this, the cells were cultured in 12-well plates, at concentration of 10^4 cells/well, in various differentiation mediums. For osteogenesis, cells were cultured for 14 days in medium consisting of DMEM-LG (Thermo Fisher Scientific), 10% FBS, 50 μg/mL ascorbate-2 phosphate (Thermo Fisher Scientific), 10^{-8} M dexamethasone (Sigma-Aldrich), and 10 mM β-glycerophosphate (Sigma-Aldrich). Alizarin Red staining (Sigma-Aldrich) was administrated to assess the mineral deposition. For adipogenesis, cells were cultured for 14 days in medium consisting of DMEM-LG,

10% FBS, 50 µg/mL ascorbate-2 phosphate, 10^{-7} M dexamethasone, and 50 µg/mL indomethacin (Sigma-Aldrich). The Cells then are stained with Oil Red O (Sigma-Aldrich) to evaluate adipogenesis. Chondrogenesis medium contained DMEM-LG, 10% FBS, 1 µM ascorbate-2 phosphate, 10^{-7} M dexamethasone, 10 ng/mL TGF-β1 (Sigma-Aldrich) and 1% sodium Pyruvate (Sigma-Aldrich). Chondrogenic differentiation was assessed by toluidine blue staining (Sigma-Aldrich) after 14 days.

2.3.2. Cell seeding and preparation of cell-scaffold constructs

PDLLA/β-TCP scaffolds at the size of 8 mm × 8 mm were fabricated with 3D printer and used for in vitro studies. A total of 5×10^5 cells were seeded into each scaffold. Cell-scaffold constructs were then incubated in stem cell growth medium in 48-well plates for the designated time according to different experimental purposes.

2.3.3. Evaluation of cell attachment

Cell attachment was evaluated using SEM (Akishima) after 5 days incubation in stem cell growth medium. Briefly, the constructs were sectioned and fixed with 1.5% glutaraldehyde (Merck) in a 0.1 M Sodium Cacodylate (CAC) (Sigma-Aldrich) buffer. Next, they were post-fixed in 1% osmium tetroxide (Sigma-Aldrich) in 0.1 M CAC buffer for another 1 h, followed by dehydrating through an ethanol series (30%–100%) and drying in hexamethyldisilazane (Sigma-Aldrich). The samples were then coated with gold and subjected to SEM imaging. Scaffolds without cells but cultured and processed under the same conditions were also examined by SEM as controls.

2.3.4. Evaluation of cell viability/proliferation

Cell proliferation/viability was evaluated after 24 h, 3 and 5 days incubation in stem cell growth medium using 3-(4,5-dimethylthiazol-2-yl)-2,5-diphenyltetrazolium bromide (MTT) (Sigma-Aldrich) and DNA counting assay. For MTT assay, cell culture mediums were replaced with fresh medium containing 10% MTT solution (5mg/ml). Then the cells were incubated for 2 h protected from light at 37°C and 5% CO2. Next, mediums were replaced with DMSO (Sigma-Aldrich) and shake to ensure complete solubilization. The optical density is read at 570 nm in ELSA reader (BioTek). For DNA counting, the constructs first washed with PBS in order to remove any dead cells and detached cells, then they were dissolved in 1ml Tryzol (Life Technologies) at room temperature for 10 min followed by phase separation using chloroform. Then, DNA was isolated by precipitation. DNA concentration was measured using Nano drop (Thermo Fisher Scientific).

Cell viability, as well as, cell attachment was also evaluated using live/dead and DAPI staining (Sigma-Aldrich) after 5 days incubation in stem cell growth medium. To do live/dead assay, the constructs were incubated with a mixture of Cell Tracker™ green (5-chloromethylfluorescein diacetate and Ethidium Homodimer (EH-1) for 1 h at room temperate. The viable cells (green fluorescence) and dead cells (red fluorescence) were detected with a fluorescence microscope. For DAPI staining, the constructs first were fixed with 4% glutaraldehyde (Merck) followed by DAPT staining for 10 s. Then cells were monitored with a fluorescence microscope.

2.3.5. Evaluation of osteogenic differentiation

The osteogenic differentiation capability of cells seeded on the constructs was also determined using Alkaline Phosphatase (ALP) activity, after 7 and 14 days induction in osteogenic medium. for ALP activity assay, constructs were rinsed with PBS and homogenized in lysis buffer (pH 7.5, 10 mMTris–HCl, 1 mM MgCl2, and 0.05% Triton X-100). The resulting mixture was then centrifuged at 12,000 rpm for 10 min at 4°C. The cell lysate was mixed with p-nitrophenol phosphate substrate solution (Sigma-Aldrich) and alkaline buffer solution (Sigma-Aldrich). After incubation at 37°Cfor 15 min, the above mixture was added to 0.5 N NaOH to stop the reaction and the absorbance at 405 nm was measured using ELISA reader (BioTek).

The osteogenic differentiation of the cells seeded on the constructs was also determined by evaluation of osteogenic markers using Real time RT-PCR. The expression of ALP, BMP2, COL I and RUNX2 was evaluated as

follows: First, constructs are dissociated with Tryzol (Life Technologies) reagent followed by RNA isolation. Then the quantity and quality of isolated RNA was determined using Nanodrop spectrometer (Thermo Fisher Scientific). RNA was reverse-transcribed into cDNA. Reverse transcription was performed at 37°C for 50 min followed by heating at 70°C for 15 min to inactivate the reaction. cDNA templates were used for SYBR Green real-time PCR to detect cycle threshold (CT) values with Applied Biosystems' Real-Time PCR System. The CT values were normalized to GAPDH to calculate ΔCT. RGE was calculated with the formula $2^{-\Delta\Delta CT}$ using the control as the reference (RGE = 1). Primer sequences are given at Table 1.

Table 1. Primer sequences used for Real-time PCR.

Primer name	Accession number	Sequences 5′-3′
ALP/F ALP/R	NM-001177520.2	AGGACGCTGGGAAATCTGTG ATGAGCTGGTAGGCGATGTC
BMP2/F BMP2/R	NM-001200.4	GGACGCTCTTTCAATGGACG AGCAGCAACGCTAGAAGACAG
COL1A1/F COL1A1/R	NM-000088.3	TGGAGCAAGAGGCGAGAG ATCACCCTTAGCACCATCG
RUNX2/F RUNX2/R	NM-001015051.3	CGGAATGCCTCTGCTGTTATG AGGATTTGTGAAGACGGTTATGG

2.3.6. Statistical analysis

All experiments was conducted in triplicated. The results are expressed as mean ± standard deviation. Two-way analysis of variance (ANOVA) were conducted in SPSS software (version 15.0; SPSS, Chicago, IL). Differences were considered with a confidence interval 95% (P value ≤ 0.05) for all analyses.

3. Results

3.1. Physicomechanical characterization

3.1.1. Microstructure analysis

Photographs of top view and lateral view the 3D printed PDLLA (Fig. 1A and B) and PDLLA/β-TCP (Fig. 1C and D) scaffolds shows that the scaffolds are porous with interconnected pores and reproducible pattern. It is worthy of note that with the designed inner structure (90° shift between layers) pores are also formed in the z-axis, which is very crucial for clinical applications as facilitates infiltration of cells to the scaffold.

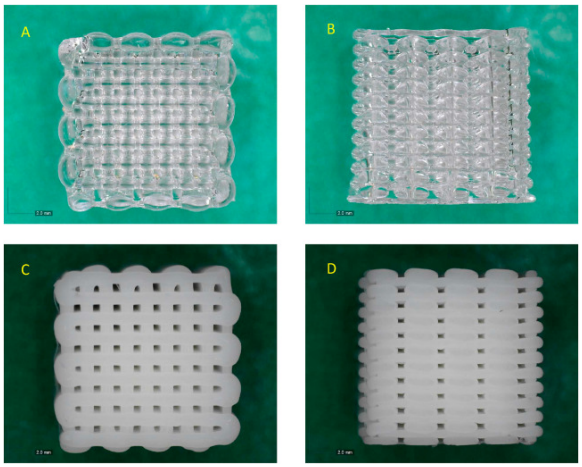

Fig. 1. Photograph of the (A) top, (B) lateral view of PDLLA scaffolds, and (C) top, (D). lateral view of PDLLA/β-TCP scaffolds printed with 3D Bioplotter (scale bar 2 mm).

The fabricated scaffolds were scanned using the LEXT OLS4000 3D Laser Measuring Microscope (Olympus). As can be seen in Fig. 2A–D, scaffolds have almost identical microstructure with smooth surface topography. The width of the pores in both PDLLA and PDLLA/ß-TCP scaffolds was measured to be 320 µm and the width of strands was found to be 400 µm. The pore size in the lateral side of scaffolds was measured to be in the range of 200–250 µm.

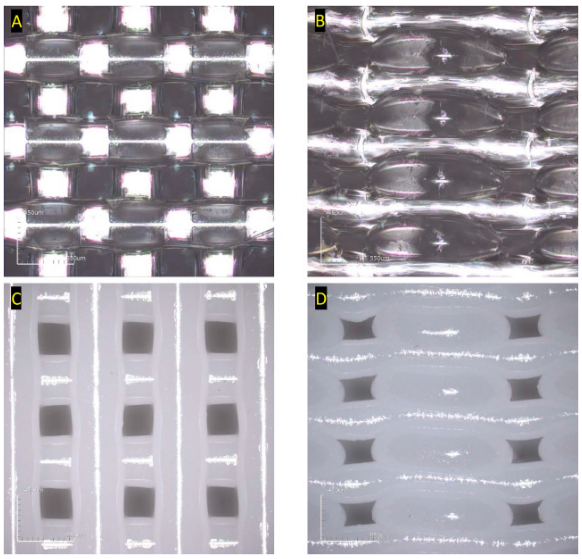

Fig. 2. Micrographs of the inner structure of (A) top, (B) lateral view of PDLLA scaffolds, and (C) top, (D) lateral view of PDLLA/ß-TCP scaffolds at 5x magnification (scale bar x: 550 µm, y: 450 µm).

3.1.2. Porosity measurement

As summarized in Table 2, porosity of PDLLA/β-TCP scaffolds were measured to be slightly higher than the 3-printed scaffolds based on pristine PDLLA. Such observation is attributed to the altered extruded melt viscosity after incorporation of β-TCP. In fact, viscosity increase originates from interaction of PDLLA chains with β-TCP particles. This effect is also evident based on differential scanning calorimetry results, which showed higher glass transition temperature for PDLLA/β-TCP compared to PDLLA. As printing condition including temperature, pressure, and speed kept constant to fabricate both PDLLA and PDLLA/β-TCP scaffolds, thinner strands were extruded for the composite formulation which resulted in relatively higher porosity. The laser microscope images confirm the thinner strands for PDLLA/β-TCP compared to pure PDLLA scaffolds.

Table 2. Porosity, Young's Modulus, and compressive strength of 3D printed scaffolds.

Scaffolds	**Porosity (%)**	**Young's modulus (MPa)**	**Compressive strength (MPa)**
PDLLA	57.1 ± 2.6	447.2 ± 53.7	24.1 ± 3.9
PDLLA/b-TCP	55.6 ± 1.5	514.5 ± 34.3	32.3 ± 2.4

3.1.3. Fourier transform infrared spectroscopy (FTIR) analysis

FTIR patterns of β-TCP, PDLLA and PDLLA/β-TCP are depicted in Fig. 3. By comparing the typical absorption bands of PDLLA and β-TCP, peaks appeared at 790 and 1500–1800 cm^{-1} that are thought to be the RCOO-Ca absorption bands. In order to reach composite scaffolds with improved mechanical properties, the interface between the PDLLA matrix and the dispersed phase i.e., β-TCP particles should be strong to enable transferring

the stress of mechanical loading from polymer to the bioceramic phase. Interactions among PDLLA chains and β-TCP particles results in improved Young's Modulus and compressive strength of composite scaffolds.

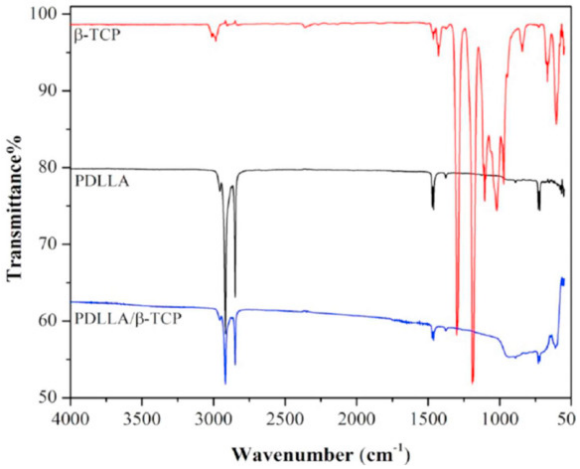

Fig. 3. FTIR spectrum of PDLLA, β-TCP powder and PDLLA/β-TCP composite.

3.1.4. Differential scanning calorimetry analysis

The thermal properties of PDLLA/β-TCP composite scaffolds were examined by differential scanning calorimetry (DSC) analysis. As shown in Fig. 4, the incorporation of β-TCP in PDLLA matrix resulted in increased glass transition temperature (T_g). The increase in Tg is a result of interactions among organic and inorganic phase in composite that cause hindered dynamic of polymer chains. This finding is well consistent with the FTIR analysis.

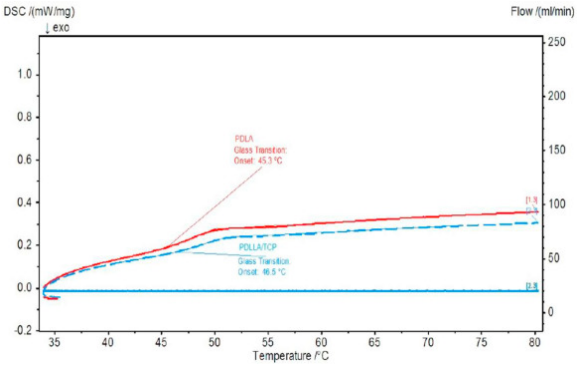

Fig. 4. The DSC thermograms of PDLLA and PDLLA/β-TCP composite scaffolds.

3.1.5. Evaluation of mechanical properties

As summarized in Table 2, PDLLA/β-TCP scaffolds exhibited increased Young's Modulus and compressive strength compared to the pristine PDLLA scaffolds. It is worthy of note that although the composite scaffolds possess higher porosity, but they showed superior mechanical strength.

3.2. BFPSC characterization according to ISCT criteria

Mesenchymal stem cell from BFP showed fibroblastic-shaped morphology (Fig. 5A). After a 3-week incubation under adipogenic conditions, BFPSCs showed the formation of neutral lipid vacuoles, visualized by staining with Oil-red O (Fig. 5B). After 14 days of incubation under chondrogenic conditions, the development of cartilage matrix from BFPSCs was shown by staining the proteoglycans with Toluidine Blue (Fig. 5C). Also, calcium deposition was shown by Alizarin red staining after 14 days induction in osteogenic medium (Fig. 5D).

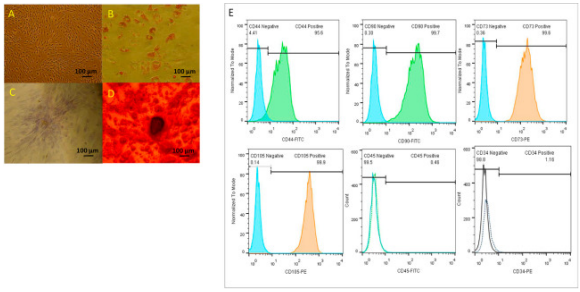

Fig. 5. BFPSC characterization according to ISCT criteria. (A–D) Multilineage differentiation capabilities of BFPSCs after 14 days in basal medium (A), adipogenic (B), chondrogenic (C) and osteogenic (D) medium. (E) Flow cytometry analysis of BFPSCs for mesenchymal stem cell surface markers.

In order to confirm whether the isolated/cultured BFPSCs display the MSC phenotype, cells were subjected to flow cytometry analysis for expression of positive CD44, CD90, CD73 and CD105 and negative (CD45 and CD34) MSC markers. The result showed that more than 95% of this cell population were positive for CD44, CD90, CD73 and CD105, MSC-surface markers, whereas they were negative for CD45 and CD34, hematopoietic markers (Fig. 5E).

3.3. Biocompatibility evaluation

3.3.1. Evaluation of cell attachment

The suitability of the 3D structure of scaffolds for cell seeding was assessed by observing cell adhesion using SEM imaging. SEM microphotographs after 5 days showed the attachment of BPSCs to the entire scaffold surface (Fig. 6C–F).

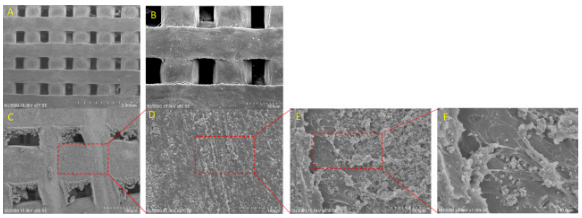

Fig. 6. BFPSC attachment on PDLLA/β-TCP. (A, B) SEM micrographs of scaffold at different magnifications. (C–F) SEM micrographs of scaffold loaded with BFPSCs after 5 day at different magnifications.

3.3.2. Evaluation of cell viability/proliferation

The proliferation/viability of BFPSCs were first monitored and quantified after 24h, 3d and 5 days by MTT and DNA counting assay (Fig. 7A and B). Both MTT and DNA counting assay showed the significant growth rate of BFSCs on scaffolds from day 1 to 5. Live-dead assay and DAPI staining were also confirmed the cell viability and attachment of BFSCs on PDLLA/β-TCP scaffold (Fig. 7C–E).

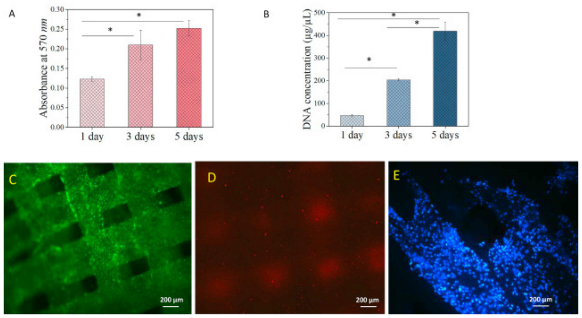

Fig. 7. BFPSC proliferation/viability on PDLLA/b- TCP. (A) MTT assay after 24h, 3d and 5d in stem cell culture medium. (B) DNA counting assay after 24h, 3d and 5d in stem cell culture medium. (C, D) Live-dead assay after 5days. (E) DAPI staining after 5days. ∗ indicates significant difference at 0.05.

3.3.3. Evaluation of osteogenic differentiation

ALP activity of BFPSCs cultured on PDLLA/β-TCP scaffold significantly increased from day 7 to day 14 in osteogenic induction medium as compared to cells cultured on PDLLA/β-TCP in basal medium (Fig. 8A). Using Real time RT-PCR the expression of four osteogenic genes, ALP, BMP2, COL I and RUNX2 has been evaluated at both early (7 days) and later stage (14 days) of osteogenic differentiation (Fig. 8B–E). The results indicate that the expression of given genes significantly increase at both time points as compared to control.

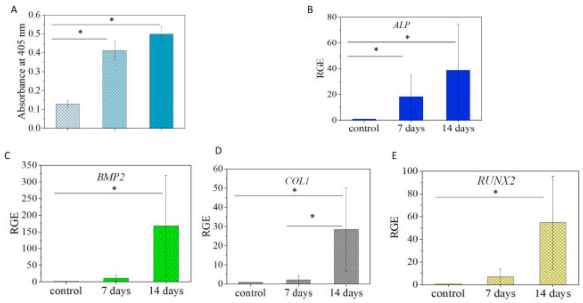

Fig. 8. Osteogenic capability of BFPSCs on PDLLA/β-TCP. (A) ALP activity assay after 5days in basal medium, 7 and 14days in osteogenic medium. (B–E) Expression of osteogenic-related markers after 5days in basal medium, 7 and 14days in osteogenic medium as determined by Real time RT-PCR. ∗ indicates significant difference at 0.05.

4. Discussion

The preparation of composite scaffolds, containing both organic and inorganic parts, close to the structure of the native bone, would help to fulfill the requirements for bone regeneration in load-bearing areas [4,5]. In this study, PDLLA/β-TCP scaffolds were fabricated using CAD and 3D print technology. Then, the physicomechanical characteristics of the customized scaffolds were investigated to see if they match with natural bone properties. Also, the in vitro biological characteristics of manufactured scaffolds in conjugation with BFPSCs in order to evaluate their biocompatibility and osteogenic differentiation capacity were evaluated.

We took advantage of using a 3D printing technology in order to manufacture scaffolds with interconnected porous structure and a regular and reproducible morphology of the pores which has been shown to be essential for continuous bone regeneration [28,29]. A part from fabricating the controlled interconnected porous structure, this technology allowed to fabrication of scaffold with pore size range of 320–400 μm. However, there is still a controversy within the literature regarding the scaffold optimal pore size for ideal bone regeneration [[28], [29], [30], [31]]. Some studies recommended higher pore size dimeter for an ideal bone ingrowth and vascularization [32,33]. However, others showed that increasing the pore diameter would significantly diminished scaffold mechanical strength [5,31,32]. A mechanical stability of a scaffold not only related to the pore size, but also significantly affected by porosity percentage [5,34]. A study by Bose et al., on different porosity of β-TCP scaffolds showed that compressive strength of the scaffolds decreased with increasing porosity percentage [35]. In this study, fabricated scaffolds have the porosity of 55% which is well-fitted to the lower range of natural cancellous bone, i.e.50–90%. However, considering the fact that fabricated scaffolds have proper mechanical properties, having the low porosity percentage of scaffolds are acceptable.

Mechanical properties of 3D-printed scaffolds are decisive on their biomechanical performance in tissue engineering. Both composition and porosity affect the mechanical features of scaffolds. Comparing the values of

strength and compressive modulus of 3D-printed scaffolds with those of for the cancellous bone (compressive strength: 2–12 MPa, compressive modulus: 50–500 MPa), reveals 3D-printed PDLLA-based scaffolds as promising matrices for cancellous bone regeneration. The composite of ceramic, β-TCP, and polymer, PDLLA, phases has been combined the desired properties of both materials [13,15,[36], [37], [38], [39], [40], [41]]. To achieve this, most studies have been used the equal ration of PDLLA and ceramic materials [[2], [3], [4], [5],17]. A study by Lin et al., has been shown that increasing TCP from 30- 50 wt% in composite scaffold improved both mechanical strength and elastic modulus [3]. However, Bae EB et al., claimed that increasing the percentage of β-TCP in a composite scaffold would increase the viscosity which significantly affects the scaffold printing speed. Hence, in order to balance between β-TCP content and printing rate, they kept the percentage of polymer phase higher [5]. Similarly, we kept the ration of polymer phase slightly higher that ceramic phase i.e., 60% PDLLA vs. 40% β-TCP, in order to have the best compromise between printing process and scaffold mechanical properties.

Degradation of PDLLA causes an acidic environment in the implantation site of the scaffold which may result in inflammatory responses. In the current research, β-TCP as a biocompatible ceramic was incorporated into the polyester scaffold to not only conduct osteogenesis, but also buffer the subsequent acidic environment in the vicinity of the composite scaffold.

As widely reported in previous studies, incorporation of β-TCP in composite scaffolds significantly enhance their mechanical properties [2,3,6]. Similarly, in this study addition of 40% β-TCP in PDLLA composite significantly increased both compressive strength and elasticity of the scaffold. In compare to study by Linder M et al., and Zhang LF et al., we used the lower ratio of β-TCP in composite scaffold (40% vs 50%) [2,6], however, higher compressive strength is achieved. Here, the comparative strength is higher than cancellous bone with a compressive strength in the range of 2–20 MPa [2]. however, compared to compressive strength of human cortical bone (70-280MPA), the fabricated scaffold still showed lower stability [4]. In several studies they reported the fabricated ceramic-polymer scaffolds with much higher mechanical strength, compared to our composite scaffold, however; they significantly compromised the scaffold porosity which is ultimately affecting the growth of new bone [5,9,23].

Apart from physicomechanical properties resembling natural bone structure, an ideal bone graft material should have proper biocompatibility and osteogenic differentiation capacity properties [5,23].

A fabricated composite material in this study has been extensively evaluated for their ability to support cellular attachment, proliferation, as well as osteogenic differentiation/induction. BFPSCs have been chosen for these analyses due to their well-documented potentials for bone tissue engineering [42,43]. Similar to previous studies [[44], [45], [46]], here in incorporation of β-TCP support both attachment and proliferation of BFPSCs loaded on composite materials. Moreover, this composite material showed the proper osteogenic differentiation capacity as confirmed by both ALP and gene expression analysis.

Further in vivo implantation of this fabricated scaffold is recommended in order to evaluate its potential for bone regeneration. Moreover, in order to translate the finding of this study in clinical setting, fabrication of this scaffold with GMP-grade materials is recommended.

5. Conclusion

Hence, the 3D printed customized scaffold in this study, with regard to proper pore size, porosity, mechanical strength, material composition, biocompatibility, and osteogenic differentiation capacity demonstrate a promising composite material for the purpose of the bone tissue engineering.

CRediT authorship contribution statement

Maryam Rezai Rad: Formal analysis, Conceptualization, Methodology, Investigation, Writing - original draft, Writing - review & editing, Visualization. **Farahnaz Fahimipour:** Investigation, Writing - original draft, Visualization. **Erfan Dashtimoghadam:** Investigation, Writing - original draft. **Hanieh Nokhbatolfoghahaei:** Formal analysis, Writing - original draft, Visualization. **Lobat Tayebi:** Resources, Validation. **Arash Khojasteh:** Conceptualization, Validation, Resources, Supervision, Acquisition of the financial support for the project leading to this publication.

Declaration of competing interest

The authors declare that they have no known competing financial interests or personal relationships that could have appeared to influence the work reported in this paper.

Acknowledgments

This study was supported by a agrant recieved from National Institute for Medical Research Development (NIMAD; Grant No.940547).

References

[1] F. Hajiali, S. Tajbakhsh, A. Shojaei. **Fabrication and properties of polycaprolactone composites containing calcium phosphate-based ceramics and bioactive glasses in bone tissue engineering: a review.** Polym. Rev., 58 (1) (2018), pp. 164-207

[2] M. Lindner, S. Hoeges, W. Meiners, K. Wissenbach, R. Smeets, R. Telle, R. Poprawe, H. Fischer. **Manufacturing of individual biodegradable bone substitute implants using selective laser melting technique.** J. Biomed. Mater. Res., 97 (4) (2011), pp. 466-471

[3] F.H. Lin, T.M. Chen, C.P. Lin, C.J. Lee. **The merit of sintered PDLLA/TCP composites in management of bone fracture internal fixation.** Artif. Organs, 23 (2) (1999), pp. 186-194

[4] L.M. Ehrenfried, D. Farrar, D. Morsley, R. Cameron. **Mechanical Behaviour of Interpenetrating Co-continuous β-TCP-PDLLA Composites, Key Engineering Materials.** Trans Tech Publ (2008), pp. 407-410

[5] R. Smeets, M. Barbeck, H. Hanken, H. Fischer, M. Lindner, M. Heiland, M. Wöltje, S. Ghanaati, A. Kolk. **Selective laser-melted fully biodegradable scaffold composed of poly (d, l-lactide) and β-tricalcium phosphate with potential as a biodegradable implant for complex maxillofacial reconstruction: in vitro and in vivo results.** J. Biomed. Mater. Res. B Appl. Biomater., 105 (5) (2017), pp. 1216-1231

[6] L.F. Zhang, R. Sun, L. Xu, J. Du, Z.C. Xiong, H.C. Chen, C.D. Xiong. **Hydrophilic poly (ethylene glycol) coating on PDLLA/BCP bone scaffold for drug delivery and cell culture.** Mater. Sci. Eng. C, 28 (1) (2008), pp. 141-149

[7] N. Ignjatović, S. Tomić, M. Dakić, M. Miljković, M. Plavšić, D. Uskoković. **Synthesis and properties of hydroxyapatite/poly-L-lactide composite biomaterials.** Biomaterials, 20 (9) (1999), pp. 809-816

[8] A. Kolk, J. Handschel, W. Drescher, D. Rothamel, F. Kloss, M. Blessmann, M. Heiland, K.-D. Wolff, R. Smeets. **Current trends and future perspectives of bone substitute materials–from space holders to innovative biomaterials.** J. Cranio-Maxillofacial Surg., 40 (8) (2012), pp. 706-718

[9] S. Bose, S. Vahabzadeh, A. Bandyopadhyay. **Bone tissue engineering using 3D printing.** Mater. Today, 16 (12) (2013), pp. 496-504

[10] H.-H. Horch, R. Sader, C. Pautke, A. Neff, H. Deppe, A. Kolk. **Synthetic, pure-phase beta-tricalcium phosphate ceramic granules (Cerasorb®) for bone regeneration in the reconstructive surgery of the jaws.** Int. J. Oral Maxillofac. Surg., 35 (8) (2006), pp. 708-713

[11] S. Henriksen, M. Ding, M.V. Juhl, N. Theilgaard, S. Overgaard. **Mechanical strength of ceramic scaffolds reinforced with biopolymers is comparable to that of human bone.** J. Mater. Sci. Mater. Med., 22 (5) (2011), p. 1111

[12] D.S. Metsger, T. Driskell, J. Paulsrud. **Tricalcium phosphate ceramic--a resorbable bone implant: review and current status.** JADA (J. Am. Dent. Assoc.), 105 (6) (1939), pp. 1035-1038. 1982

[13] S. Samavedi, A.R. Whittington, A.S. Goldstein. **Calcium phosphate ceramics in bone tissue engineering: a review of properties and their influence on cell behavior.** Acta Biomater., 9 (9) (2013), pp. 8037-8045

[14] R.Z. LeGeros. **Calcium phosphate-based osteoinductive materials.** Chem. Rev., 108 (11) (2008), pp. 4742-4753

[15] J.E. Davies, R. Matta, V.C. Mendes, P.S. Perri de Carvalho. **Development, characterization and clinical use of a biodegradable composite scaffold for bone engineering in oro-maxillo-facial surgery.** Organogenesis, 6 (3) (2010), pp. 161-166

[16] J. Taboas, R. Maddox, P. Krebsbach, S. Hollister. **Indirect solid free form fabrication of local and global porous, biomimetic and composite 3D polymer-ceramic scaffolds.** Biomaterials, 24 (1) (2003), pp. 181-194

[17]C. Gayer, J. Abert, M. Bullemer, S. Grom, L. Jauer, W. Meiners, F. Reinauer, M. Vučak, K. Wissenbach, R. Poprawe. **Influence of the material properties of a poly (D, L-lactide)/β-tricalcium phosphate composite on the processability by selective laser sintering.** J.Mech. Behav.Biomed. Mater., 87 (2018), pp. 267-278

[18] J. Abert, A. Amella, S. Weigelt, H. Fischer. **Degradation and swelling issues of poly-(d, l-lactide)/β-tricalcium phosphate/calcium carbonate composites for bone replacement.** J.Mech. Behav.Biomed. Mater., 54 (2016), pp. 82-92

[19] A.M. Haaparanta, S. Haimi, V. Ellä, N. Hopper, S. Miettinen, R. Suuronen, M. Kellomäki. **Porous polylactide/β-tricalcium phosphate composite scaffolds for tissue engineering applications.** J. Tissue.Eng. Regen. Med., 4 (5) (2010), pp. 366-373

[20] R.C.d.A.G. Mota, E.O. da Silva, F.F. de Lima, L.R. de Menezes, A.C.S. Thiele. **3D printed scaffolds as a new perspective for bone tissue regeneration: literature review.** Mater. Sci. Appl., 7 (8) (2016), pp. 430-452

[21] K. Ji, Y. Wang, Q. Wei, K. Zhang, A. Jiang, Y. Rao, X. Cai. **Application of 3D printing technology in bone tissue engineering.** Bio-Design.Manuf, 1 (3) (2018), pp. 203-210

[22] C. Wang, W. Huang, Y. Zhou, L. He, Z. He, Z. Chen, X. He, S. Tian, J. Liao, B. Lu. **3D printing of bone tissue engineering scaffolds.** Bioactive Materials, 5 (1) (2020), pp. 82-91

[23] I.S. Deschamps, G.L. Magrin, R.S. Magini, M.C. Fredel, C.A. Benfatti, J.C. Souza. **On the synthesis and characterization of β-tricalcium phosphate scaffolds coated with collagen or poly (D, L-lactic acid) for alveolar bone augmentation.** Eur. J. Dermatol., 11 (4) (2017), pp. 496-502

[24] V. Karageorgiou, D. Kaplan. **Porosity of 3D biomaterial scaffolds and osteogenesis.** Biomaterials, 26 (27) (2005), pp. 5474-5491

[25] Q.L. Loh, C. Choong. **Three-dimensional scaffolds for tissue engineering applications: role of porosity and pore size.** Tissue Eng. B Rev., 19 (6) (2013), pp. 485-502

[26]M. Rasoulianboroujeni, F. Fahimipour, P. Shah, K. Khoshroo, M. Tahriri, H. Eslami, A. Yadegari, E. Dashtimoghadam, L. Tayebi. **Development of 3D-printed PLGA/TiO2 nanocomposite scaffolds for bone tissue engineering applications.** Mater. Sci. Eng. C, 96 (2019), pp. 105-113

[27] F. Zhao, Y. Yin, W.W. Lu, J.C. Leong, W. Zhang, J. Zhang, M. Zhang, K. Yao. **Preparation and histological evaluation of biomimetic three-dimensional hydroxyapatite/chitosan-gelatin network composite scaffolds.** Biomaterials, 23 (15) (2002), pp. 3227-3234

[28] A.C. Jones, C.H. Arns, A.P. Sheppard, D.W. Hutmacher, B.K. Milthorpe, M.A. Knackstedt. **Assessment of bone ingrowth into porous biomaterials using MICRO-CT.** Biomaterials, 28 (15) (2007), pp. 2491-2504

[29] P. Habibovic, U. Gbureck, C.J. Doillon, D.C. Bassett, C.A. van Blitterswijk, J.E. Barralet. **Osteoconduction and osteoinduction of low-temperature 3D printed bioceramic implants.** Biomaterials, 29 (7) (2008), pp. 944-953

[30]A. Fukuda, M. Takemoto, T. Saito, S. Fujibayashi, M. Neo, D.K. Pattanayak, T. Matsushita, K. Sasaki, N. Nishid a, T. Kokubo. **Osteoinduction of porous Ti implants with a channel structure fabricated by selective laser melting.** Acta Biomater., 7 (5) (2011), pp. 2327-2336

[31] M.I. Gariboldi, S.M. Best. **Effect of ceramic scaffold architectural parameters on biological response.** Front. Bioeng.Biotechnol., 3 (2015), p. 151

[32] S. Van Bael, Y.C. Chai, S. Truscello, M. Moesen, G. Kerckhofs, H. Van Oosterwyck, J.-P. Kruth, J. Schrooten. **The effect of pore geometry on the in vitro biological behavior of human periosteum-derived cells seeded on selective laser-melted Ti6Al4V bone scaffolds.** Acta Biomater., 8 (7) (2012), pp. 2824-2834

[33] W.D. Holder Jr., H.E. Gruber, A.L. Moore, C.R. Culberson, W. Anderson, K.J. Burg, D.J. Mooney. **Cellular ingrowth and thickness changes in poly-l-lactide and polyglycolide matrices implanted subcutaneously in the rat.** J. Biomed. Mater. Res.: Off. J. Soc.Biomater. Jpn.Soc.Biomater.Aust. Soc.Biomater., 41 (3) (1998), pp. 412-421

[34] M. Seidenstuecker, S. Lange, S. Esslinger, S.H. Latorre, R. Krastev, R. Gadow, H.O. Mayr, A. Bernstein. **Inversely 3D-printed β-TCP scaffolds for bone replacement.** Materials, 12 (20) (2019), p. 3417

[35] A. Bruyas, F. Lou, A.M. Stahl, M. Gardner, W. Maloney, S. Goodman, Y.P. Yang. **Systematic characterization of 3D-printed PCL/β-TCP scaffolds for biomedical devices and bone tissue engineering: influence of composition and porosity.** J. Mater. Res., 33 (14) (2018), pp. 1948-1959

[36] S. Bose, J. Darsell, M. Kintner, H. Hosick, A. Bandyopadhyay. **Pore size and pore volume effects on alumina and TCP ceramic scaffolds.** Mater. Sci. Eng. C, 23 (4) (2003), pp. 479-486

[37] P.X. Ma. **Scaffolds for tissue fabrication.** Mater. Today, 7 (5) (2004), pp. 30-40

[38] Y. Liu, J. Lim, S.-H. Teoh. **Development of clinically relevant scaffolds for vascularised bone tissue engineering.** Biotechnol. Adv., 31 (5) (2013), pp. 688-705

[39] R.A. Horowitz, Z. Mazor, R.J. Miller, J. Krauser, H.S. Prasad, M.D. Rohrer. **Clinical evaluation alveolar ridge preservation with a beta-tricalcium phosphate socket graft.** Comp. Cont. Educ. Dent., 30 (9) (2009), pp. 588-590

[40] X. Miao, D.M. Tan, J. Li, Y. Xiao, R. Crawford. **Mechanical and biological properties of hydroxyapatite/tricalcium phosphate scaffolds coated with poly (lactic-co-glycolic acid).** Acta Biomater., 4 (3) (2008), pp. 638-645

[41] Y. Kang, A. Scully, D.A. Young, S. Kim, H. Tsao, M. Sen, Y. Yang. **Enhanced mechanical performance and biological evaluation of a PLGA coated β-TCP composite scaffold for load-bearing applications.** Eur. Polym. J., 47 (8) (2011), pp. 1569-1577

[42] M.-H. Lee, C. You, K.-H. Kim. **Combined effect of a microporous layer and type I collagen coating on a biphasic calcium phosphate scaffold for bone tissue engineering.** Materials, 8 (3) (2015), pp. 1150-1161

[43] I. Yip, L. Ma, N. Mattheos, M. Dard, N.P. Lang. **Defect healing with various bone substitutes.** Clin. Oral Implants Res., 26 (5) (2015), pp. 606-614

[44] M. Rezai Rad, M. Bohloli, M. Akhavan Rahnama, A. Anbarlou, P. Nazeman, A. Khojasteh. **Impact of tissue harvesting sites on the cellular behaviors of adipose-derived stem cells: implication for bone tissue engineering.** Stem Cell. Int., 2017 (2017)

[45] H. Nokhbatolfoghahaei, M. Bohlouli, Z. Paknejad, M.R. Rad, L.M. Amirabad, N. Salehi-Nik, S. Shahriari, N. Nadjmi, A. Ebrahimpour, A. Khojasteh. **Bioreactor cultivation condition for engineered bone tissue: effect of various bioreactor designs on extra cellular matrix synthesis.** J. Biomed. Mater. Res., 108 (8) (2020), pp. 1662-1672

[46] J.-H. Shim, T.-S. Moon, M.-J. Yun, Y.-C. Jeon, C.-M. Jeong, D.-W. Cho, J.-B. Huh. **Stimulation of healing within a rabbit calvarial defect by a PCL/PLGA scaffold blended with TCP using solid freeform fabrication technology.** J. Mater. Sci. Mater. Med., 23 (12) (2012), pp. 2993-3002